

Rapid Discrimination of Resident Space Objects Using Near-Infrared Photometry

Eric C. Pearce*, Harrison Krantz*, Adam Block*, Brad Sease†, Mitchell Kirshner‡

**Steward Observatory, University of Arizona*

†Computational Physic Inc.

‡University of Arizona System and Industrial Engineering

ABSTRACT

The characterization of deep space debris poses a significant challenge in Space Situational Awareness (SSA). To be most useful, characterization should provide actionable information quickly, even under non-ideal observing conditions. Multi-color photometry and the resultant color indices offer the potential to rapidly discriminate between debris and intact space objects such as rocket bodies and satellites. These multi-color techniques can also identify anomalous members of object groups and cue higher fidelity data collections and studies.

In this paper, we present the results from our 2020–2021 measurements campaign supplemented by further analysis from our previous 2016–2017 campaign. In 2017-2018, our team began developing and demonstrating rapid multi-color photometry techniques using the Russian SL-12 fourth stage rocket bodies (RB). We demonstrated that anomalous members of our rocket body cohort can be readily identified using only near-infrared (IR) color indices. During late 2020 and early 2021, our team expanded our previous characterization by using both the United Kingdom Infrared Telescope (UKIRT) Wide Field Camera (WFCAM) and the 1–5 μm Imager-Spectrometer (UIST). Specifically, we have expanded our data set to include:

- (a) more SL-12 fourth stage RBs increasing years-on-orbit sampling from our 2016-2017 campaign,
- (b) Centaur RBs of the same type as the returning RB cataloged as Near-Earth Object 2020 SO,
- (c) a selection of Molniya communication satellites including the -1K, 1T, -2, and -3 variants,
- (d) Russian FREGAT and SL-6 upper stage RBs in Molniya orbits,
- (e) intact payloads selected from satellites using the Boeing HS-376 busses.

Our new data set provides us with overlapping broadband IR colors and high-resolution spectra in those same color bands. We carefully chose our targets to include a mix of objects with known compositions to allow the development and evaluation of novel techniques to interpret our broadband near-IR photometry. The addition of Molniya payloads and RBs is a unique addition to existing literature since all previously published studies have focused on objects in geosynchronous orbits. For the first time, we can analyze near-IR photometry with the context of the full resolution near-IR spectra of same-type. We offer insight into refining the spectral bands of interest for characterization and provide an approach to improve rapid discrimination capabilities using substantially more efficient near-IR photometric techniques.

1. INTRODUCTION

Since the launch of Sputnik in 1957, space surveillance has tracked and studied satellites and space debris with optical telescopes. The first attempts to use optical photometry to characterize satellites were published by the U.S and Russians in the late 1950s [1, 2]. The excellent historical review papers by Lambert [3] and Sukhov [4] summarize much of the history of photometric technique development in the US and Russia respectively. Multi-color photometric measurements offer the opportunity to quickly measure the bulk spectral characteristics of a space object. The concept of exploiting the color indices in the visible bands has been previously explored in SSA. For example, Lederer et al. used BVRI photometry from the Cerro Tololo Inter-American Observatory (CTIO) 0.9 m telescope to compare measured color indices of 18 IDCSP (Initial Defense Communications Satellite Program) satellites with the predictions from laboratory measurements of solar cells [5]. Frith et al. previously measured a selection of objects with UKIRT WFCAM and documented phase angle variation on the J-K and H-K color indices.

Phase angle variations in J-K and H-K scaled order of 0.2 to 0.3 magnitudes, and although the satellites shared some common trends, each displayed its own unique characteristic [6].

During late 2020 and early 2021, our team using the United Kingdom Infrared Telescope (UKIRT) Wide Field Camera (WFCAM) expanded upon our previous 2016–2017 characterization survey [7]. Specifically, we expanded our data set to include:

- (a) more SL-12 fourth stage RBs increasing years-on-orbit sampling from our 2016-2017 campaign,
- (b) Centaur RBs of the same type as the returning RB cataloged as Near-Earth Object 2020 SO,
- (c) a selection of Molniya communication satellites including the -1K, 1T, -2, and -3 variants,
- (d) Russian FREGAT and SL-6 upper stage RBs in Molniya orbits,
- (e) intact payloads selected from satellites using the Boeing HS-376 busses.

The 3.8 m United Kingdom InfraRed Telescope (UKIRT) is the largest dedicated IR telescope located on Mauna Kea in HI. The telescope has a suite of astronomical spectrographs and imagers operating at the Cassegrain focus, and a unique large mosaic near-IR survey camera (Wide Field CAMera; WFCAM) that operates at the prime focus [8]. WFCAM is a unique survey instrument, using a mosaic of four Rockwell Hawaii-II 2048×2048 HgCdTe imagers. For most of our photometric observations, we use an observing protocol that cycles through the standard astronomical bands from Z to K. Typical integration times are 5 s in Z, Y, J, and H, and 10 s in K. A final redundant collection in the Z band allows measurement of phase angle variation during the collection sequence that typically takes 8–10 minutes. The UKIRT control system features a robust queue scheduler and allows data collection on satellites using standard two-line element sets (TLEs).

In this paper we focus on our recent results with the HS-376 busses, highlighting the ability of near-IR photometry to distinguish between the subtle differences in solar panel material between different models. These initial results also highlight some of the challenges of applying UKIRT and near-IR photometry for SSA characterization, including deconvolving the various factors such as phase angle, rotation, and pose that all effect both color and brightness during the collection.

2. NEAR-IR PHOTOMETRY PROCESSING PIPELINE

In support of this effort, we developed an independent photometric calibration and processing pipeline for WFCAM measurements. This gives us complete insight into the techniques and ability to tailor processing techniques to our special requirements. The pipeline facilitates associating satellite photometric collections with the most relevant sidereal calibration frames and produces quick-look light curves for preliminary analysis (see Figure 1).

Our image processing pipeline utilizes PHOTOMETRYPIPELINE with some additional software [9]. The PHOTOMETRYPIPELINE software was created by Michael Mommert at Northern Arizona University for non-sidereal moving asteroids and was readily customized for satellite photometry. For our observations the telescope tracks the satellites resulting in streaked stars making differential photometry with background stars difficult or impossible to do. Thus, we made paired observations of the non-sidereal satellite and a nearby reference star field. The pairs of images are both processed with PHOTOMETRYPIPELINE, but are done separately. The sidereal reference star images are processed to calculate the zero point for the observation. The non-sidereal images are processed to calculate the instrumental magnitudes of the target satellite. All images are reduced before processing using standard practices of dark subtraction and flat-field division. During processing, images are reviewed and some tagged for rejection if there are issues such as saturation or overlapping background stars. After processing, all measurements are compiled in a SQLite database and are coupled with ephemeris information calculated from contemporaneous TLEs. We calculate the final calibrated magnitude for each target observations using the instrumental magnitude and zero point determined by a model derived from the best zero point measurements of the night. Our pipeline makes extensive use of the open-source software libraries Astropy [10,11] and Skyfield [12].

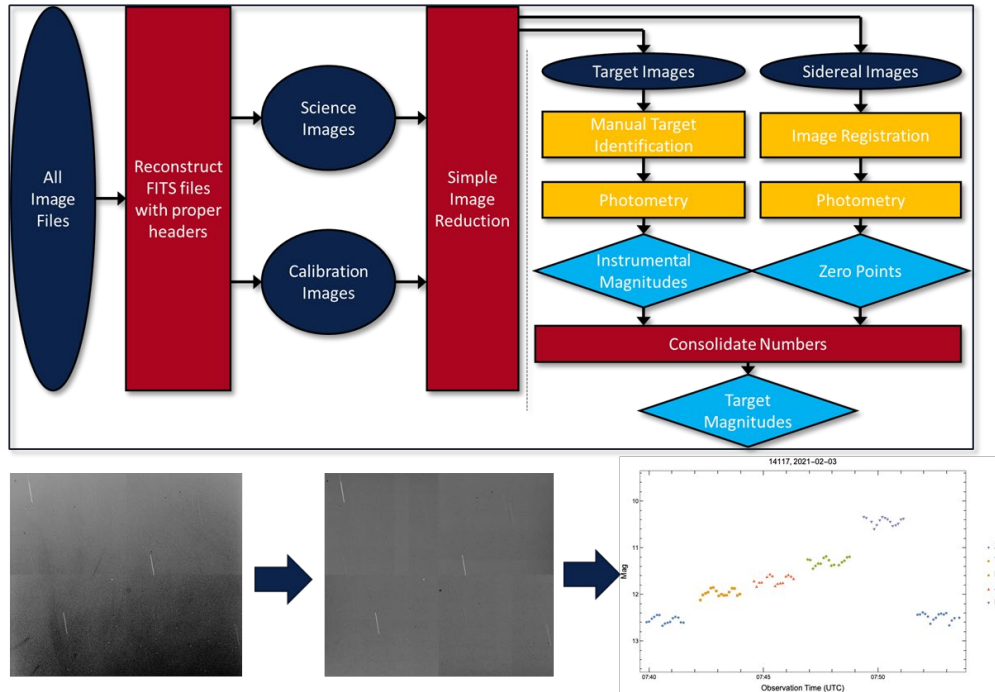


Figure 1. WFCAM Near-IR Photometric Processing Pipeline.

3. STUDY TARGET ENSEMBLES

For our survey program, we focused on three ensembles of objects that serve as known test cases of objects with similar characteristics. Our current ensembles include:

- HS-376 satellite buses. 58 satellites based on the HS-376 bus were launched over a 23-year period. There are four sub-models with slightly different cylinder geometries [13]. The cylindrical surface is covered with solar panels. Depending on the year the satellite was assembled, these solar panels may be one of five different material configurations, and in some cases hybrids of two different materials, each with unique reflectance spectra. To date, we have collected 5-color near-IR photometry on 43 different HS-376 satellites, and 2 on the similar HS-306 and HS-393 cylindrical busses.
- The SL-12 fourth stage rocket bodies. This upper stage was the mainstay of many Russian GEO launches from 1974 to 1994 [14,15]. The SL-12 was the subject of our prior investigations with both near-IR color discrimination [7], and on-orbit aging with visible spectra with the MMT telescope [16]. Recently we greatly expanded our phase angle age on-orbit sampling of this ensemble and these studies will be the subject of a future paper.
- Centaur D rocket bodies. The Centaur upper stage was first developed in late 1950s and first launched in 1963. The Centaur was most often used in different configurations on the Atlas booster [17,18]. The upper stage had multiple variations and both a single and a dual nozzle configuration. Most Centaur D upper stages were disposed in geosynchronous transfer orbit (GTO) with the earlier launches having a high enough perigee that many are still on-orbit today. Some were used for lunar insertions and remain in heliocentric orbits, including the recent apparition of “asteroid” 2020 SO which is now believed to be the upper stage used in the 1966 Surveyor 2 mission [19]. To date, we have collected 5-color photometry on 16 different Centaur-D upper stages.

3.1 BOEING HS-376 SATELLITE BUS

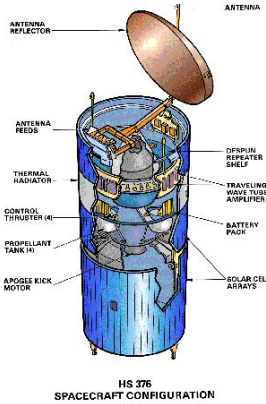


Figure 2. Drawing of the HS-376 satellite bus.

The HS-376 satellite bus was a common communications satellite bus introduced in 1978. A total of 58 HS-376 based satellites were launched from 1978 to 2003. The satellite bus features a cylindrical body with two sections one of which nests inside the other and extends out when in orbit (see Figure 2). The cylindrical body is 2.2 m in diameter and when extended between 6.5 m and 7 m long. The exterior surface is almost completely covered in solar cells and is otherwise largely featureless. The main body of the spacecraft is spin-stabilized at 50 rpm and the payload shelf despun to provide radio antenna pointing. At end-of-life the spin-rate is no longer maintained and the despun section becomes coupled with the rest of the satellite. The transfer of inertia from the body to the previously despun mass results in a reduction of the overall spin rate compared to the operational spin rate.

There are four major variations to the design of the HS-376: the standard HS-376, the long-life HS-376L, the higher-powered HS-376HP, and the larger HS-376W. Only the HS-376W featured a notably different bus with a larger diameter cylindrical body. Only four of the HS-376W were launched. During the twenty-year evolution of the HS-376, the solar cell technology was incrementally upgraded for new satellites.

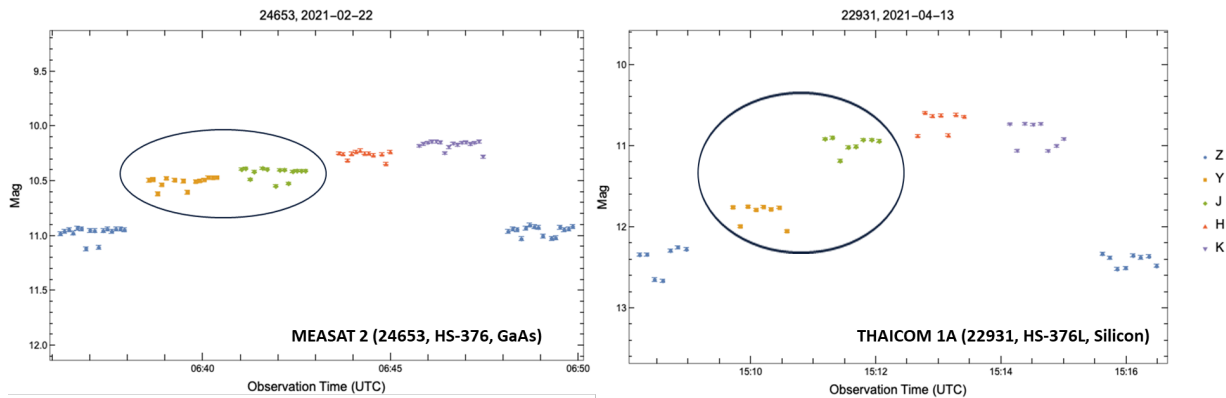


Figure 3. Comparison of GaAs (left) and Si (right) solar panels. Silicon panels have an abrupt change in reflectance near 1.1 μm , causing a characteristically high Y-J color index.

We studied the few published spectra of satellites on-orbit in the near-IR and found these wavelengths are highly diagnostic for satellite characterization. For example, the strong spectral features typically associated with solar cell band gaps in the 1.0–1.1 μm (cf. Figure 2 in [20]) and the strong features in the reflectance spectra of Kapton near 0.5 μm (c.f. Figure 3 in [21]) — both common satellite materials strongly influence red and near-IR color indices. The Z–Y and Z–J color indices are especially diagnostic of solar panel dominated space objects. In the visible part of the spectrum, the Sloan i' (695–844 nm), z_s ¹ (826–920 nm), z' (> 820 nm), and Y (950–1058 nm) offer similar diagnostic features. In particular, the sharp transition in reflectance of the older silicon solar panels has a high Y-J color index shown in Figure 3, which compares the spectral signature of THAICOM 1A (silicon), to MEASAT 2 (GaAs). Our quick-look format shows the sequential collections in Z, Y, J, H, and K, and the final collection in Z. This format allows us to quickly estimate the color indices by the discontinuities between the bands and visualize the amount of residual rotational signature that is not averaged out or is aliasing with the

¹ Here z_s refers to the Astrodon filter which cuts off the open-ended Sloan z at 920 nm.

integration time. Finally, repeating the collection in the Z band allows an estimate of the amount of variation due to changes in phase angle or range during the collection sequence.

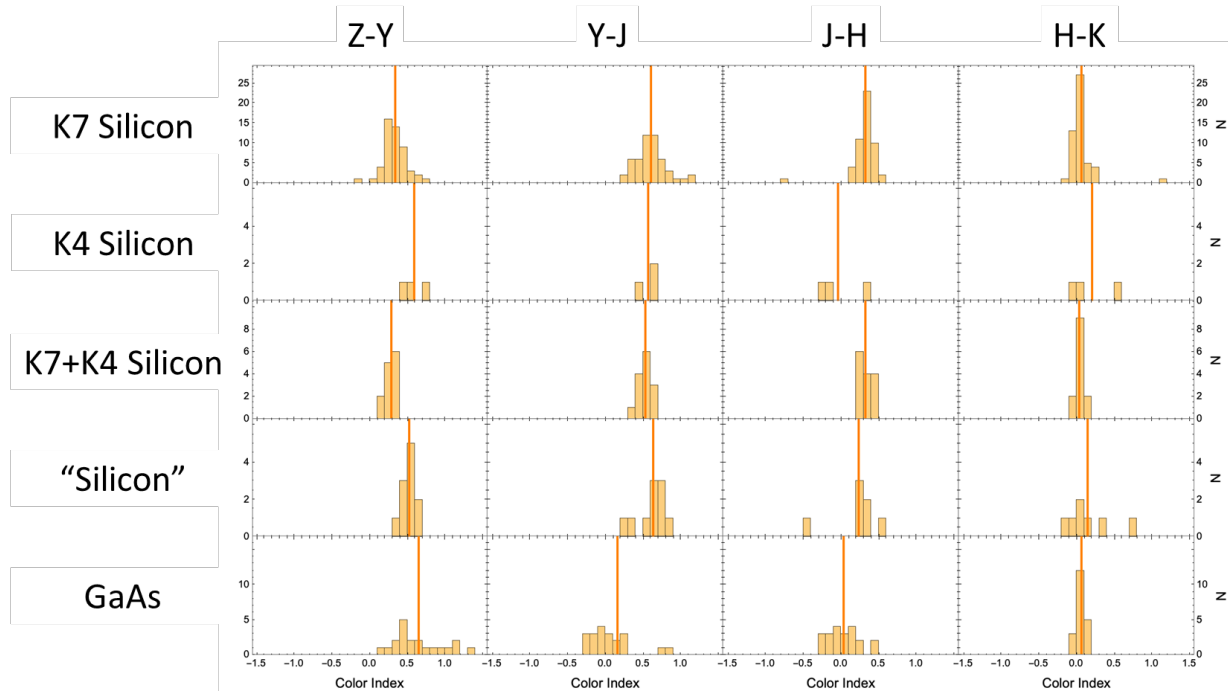


Figure 4. Color Indices of HS-376 as a function of solar panel type.

The specific solar panels each HS-376 based satellite used can be deduced based on the date they were manufactured, and many are documented by Gunter [13]. Four different specifications of solar cells were used, with the earliest HS-376 busses using shallow function n/p silicon cells, and later models using GaAs/Ge single junction and GaInP₂/GaAs/Ge dual junction panels. Reflectance spectra for only two of these four generations of solar cells have been published in the open literature. Additionally, some HS-376 satellites used a hybrid configuration of K4 and K7 shallow junction cells. Of these five different configurations, Frith et al. only observed three [6]. Figure 4 shows the distribution of near-IR color indices of our ensemble of HS-376 measurements to date. As expected, the color indices that span the solar panel band gap, especially Z-Y and Y-J, are diagnostic of the type of solar panel.

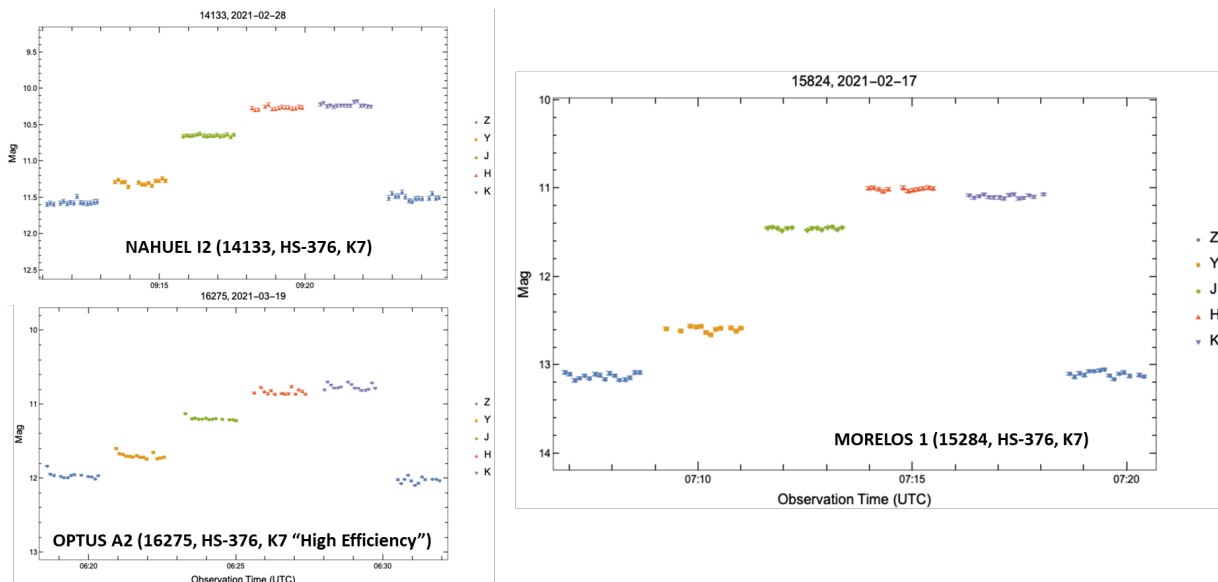


Figure 5. Anomalous H-K color index of Morelos 1 compared to other K7 solar panels.

The relatively slow filter/band change and long integration times with WFCAM complicates these measurements. We do observe some phase angle variation in color indices, and we are investigating how to back out the phase dependent variation from variations caused by the different materials and aging.

In some cases, anomalous color indices are observed despite our best expectations. For example, Figure 5 shows the quick-look presentation for Morelos 1 compared to other HS-376 busses of the era populated with K7 solar cells. Note the larger Y-J color and anomalous H-K color index. Morelos 1 and 2 used a custom antenna system tailored to the needs of the Mexico and was the first to use a planar array [23]. We speculate that the anomalous spectra of Morelos 1 may be due to the planar array. Another explanation could be variations in cover glasses and coatings associated with the development of the solar panels at the time. We expect UIST spectral collections in 2022 will lend additional insight into these differences.

3.2 CENTAUR-D UPPER STAGE

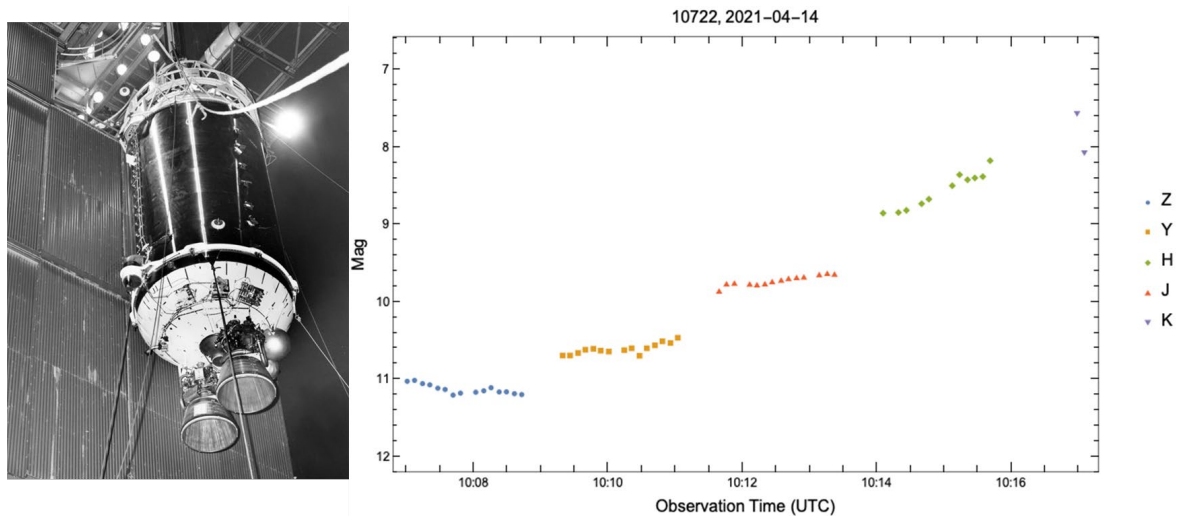


Figure 6. Typical 5-color signature of a Centaur-D rocket body. Photo NASA/JPL.

Centaur-D rocket bodies offer another interesting ensemble of test objects for development of techniques to exploit the near-IR photometry. The Centaur-D upper stages were assembled around pressure stabilized stainless steel propellant tanks and had versions with one and two nozzles. The optical signature is dominated by the stainless-steel tanks, and the spherical front and rear shrouds. We have yet to determine the surface treatments on the stainless-steel surfaces, as this appears to have evolved over the course of the program. The Centaur-Ds were disposed of in GTO orbit, with the earlier launches having a high enough perigee that they are still on orbit today. Others were used for translunar missions and disposed of heliocentrically, as was the case with the 1966 Surveyor 2 mission which recently returned as near-Earth object 2020 SO.

Overall, the rotationally averaged near-IR signature (see Figure 6) has significantly higher Z-J (~1.4) than similar era SL-12 RB Z-J (~0.75). However, interpretation of the Centaur-Ds is complicated by range dependent effects (the example shown in Figure 6 is in a high perigee 700×36,232 km orbit), and by large rotational variation. In preparation for the recent 2020 SO aberration, our team took high speed visible band photometry on several Centaur-D rocket bodies as well as 2020 SO. The typical Centaur-D had a relatively high spin rate, with periods ranging averaging near 10 s with two asymmetric peaks per rotation, and a characteristic secondary specular

feature.² Since the rotational period is very close to our integration time with the UKIRT WFCAM, the interpretation of the WFCAM photometry is complicated.

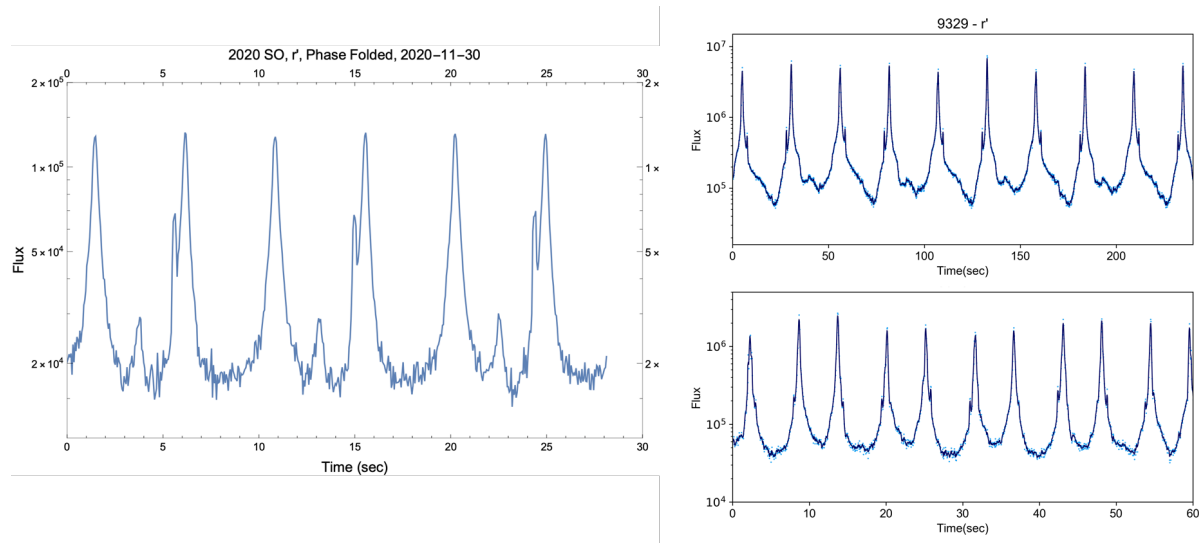


Figure 7. Visible band photometry of three different Centaur-D upper stage rocket bodies, including the upper stage mis-identified as “asteroid” 2020 SO.

4. SUMMARY AND FUTURE OBSERVATIONS

During 2021, we greatly expanded our data set of satellite and space debris 5-color near-IR photometry. Our survey used ensembles of similar known objects, such as the SL-12 and Centaur-D rocket bodies, and the Hughes HS-376 cylindrical payloads to allow us to develop techniques and interpret the efficacy of near-IR photometry for SSA characterization and discrimination. We also expanded our survey to a broader set of objects and phase angles creating what we believe is the largest near-IR photometric database of space objects. In support of this work, we developed a sophisticated data processing pipeline to allow independent processing. This pipeline processes raw WFCAM frames and associated sidereal calibration frames into calibrated 5-color magnitudes and light curves for analysis. Having a native capability to process data allows us to tailor the pipeline to the specific and unique needs of satellite characterization.

In 2022 we plan to perform new observations in the near-IR with the UKIRT 1-5 μm Imager-Spectrometer (UIST) [27]. The UIST is a unique imaging spectrometer with a 1024×1024 InSb array. UIST is designed to quickly change between imaging and spectroscopic modes and is an ideal instrument for satellite spectrometry. The UIST has several different slit/grism configurations that will allow the team to tailor collection protocols depending on the satellite brightness, desired resolution, and spectral range of interest. The combination of high-resolution spectroscopy with corresponding photometry will be a powerful tool to inform our interpretation of multi-color photometry collected with the WFCAM.

5. ACKNOWLEDGEMENTS

This work was funded by the United States Naval Observatory in support of ongoing research and development in the area of orbital debris detection and tracking, and by the University of Arizona Office of Research, Discovery and Innovation.

² Note that Figure 7 also shows the phase folded optical light curve of 2020 SO, which shows the same characteristic light curve of other Centaur-D rocket bodies. This is strong verification that 2020 SO is likely the Centaur-D rocket body associated with the Surveyor 2 launch. These results will be the subject of a future paper.

Some observations reported here were obtained with the Kuiper 61" Telescope operated by the University of Arizona Steward Observatory. The Chimera Photometer was developed with funding the University of Arizona Office of Research, Discovery and Innovation

6. REFERENCES

1. J. G. Moore, "Photometric Observations of the Second Soviet Satellite (1957 β 1)," *Publications of the Astronomical Society of the Pacific*, vol. 71, (419), pp. 163–165, 1959.
2. V. M. Grigorevskij, "About Methods of Photometry of Artificial Earth's Satellites," *Byulleten' Stantsii Nablyudeniya ISZ*, No. 7, p. 14, 1959.
3. J. V. Lambert and K.E. Kissell, "The Early Development of Satellite Characterization Capabilities at the Air Force Laboratories," in *Proceedings AMOS Conference*, Wailea, Maui, Hawaii, 2006.
4. P. P. Sukhov and K. P. Sukhov, "On some problems of photometric identification of geostationary satellites," *Kinematics and Physics of Celestial Bodies*, vol. 31, (6), pp. 314–318, 2015.
5. S.M. Lederer *et al*, "Preliminary Characterization of IDCSF Spacecrafts through a Multi-Analytical Approach," in *Proceedings AMOS Conference*, Wailea, Maui, Hawaii, 2012.
6. J. Frith, P. Anz-Meador, S. Lederer, H. Cowardin, and B. Buckalew (2015), "NIR Color vs Launch Date: A 20-year Analysis of Space Weathering Effects on the Boeing 376 Spacecraft," *Proceedings AMOS Conference*, Maui HI, September 2017.
7. E.C. Pearce *et al*. (2017), "Rapid Characterization of Geosynchronous Space Debris with 5-Color Near-IR Photometry," *Proceedings AMOS Conference*, Maui HI, September 2017.
8. M. Casali *et al*, "The UKIRT Wide-field Camera," *Astronomy and Astrophysics*, vol. 467, (2), pp. 777-784, 2007.
9. Mommert, M. "PHOTOMETRYPIPELINE: An Automated Pipeline for Calibrated Photometry." *Astronomy and Computing*, v. 18, pp. 47-53, 2017.
10. Astropy Collaboration, "The Astropy Project: Building an inclusive, open-science project and status of the v2.0 core package," *Astronomical Journal*, v. 156, no. 3, 2018.
11. Astropy Collaboration, "Astropy: A community Python package for astronomy," *Astronomy and Astrophysics*, v. 558, 2013.
12. B. Rhodes, "Skyfield: High precision research-grade positions for planets and Earth satellites generator," *Astrophysics Source Code Library*, 2019.
13. Gunter's Space Page, "Hughes/Boeing: HS-376/BSS-376," https://space.skyrocket.de/doc_sat/hs-376.htm, 2020.
14. "Mission Overview GE-6 Launch on the Proton Launch Vehicle," *International Launch Services*, 2000.
15. Gunter's Space Page, "Blok-D," http://space.skyrocket.de/doc_stage/blok-d.htm, 2020.
16. E. C. Pearce *et al*. (2019), "Examining the Effects of On-Orbit Aging of SL-12 Rocket Bodies using Visible Band Spectra with the MMT Telescope and 5-Color Photometry with the UKIRT/WFCAM," *Processing AMOS Conference*, Maui HI, September 2019.
17. V.P. Dawson and M.D. Bowles, "Taming Liquid Hydrogen: The Centaur Upper Stage Rocket 1958-2002," *NASA History Series*, NASA Office of External Relations, Washington D.C. 2004.

18. T.J. Rudman and K.L. Austad, "The Centaur Upper Stage Vehicle," *4th International Conference on Launcher Technology, Space Launcher Liquid Propulsion*, Liege, Belgium, 3-6 December 2002.
19. NASA JPL, "Earth May Have Captured a 1960s-Era Rocket Booster," <https://www.nasa.gov/feature/jpl/earth-may-have-captured-a-1960s-era-rocket-booster>, 12 November 2020.
20. K. J. Abercromby, P. Abell, and E. Baker, "Reflectance Spectra Comparison of Orbital Debris, Intact Spacecraft, and Intact Rocket Bodies in the GEO Regime," *Fifth European Conference on Space Debris*, Darmstadt, Germany, 2009.
21. L. Bai *et al*, "Spectral Scattering Characteristics of Space Target in Near-UV to Visible Bands," *Optical Express* vol. 22, (7), pp. 8515–8524, 2014.
22. M. Casali *et al*, "The UKIRT Wide-field Camera," *Astronomy and Astrophysics*, vol. 467, (2), pp. 777-784, 2007.
23. Gunter's Space Page, "Morelos 1, 2," https://space.skyrocket.de/doc_sdat/morelos-1.htm
24. W.G. Grant (2018), "The MMT Observatory: Entering a New Era of Scientific Discovery," *Proceedings of the SPIE, Ground-based and Airborne Telescopes VII*, Vol. 10700, id. 107002T, 6 July 2018.
25. J.R.P. Angel, R.L Hilliard, and R.J. Weymann (1979), *SAO Special Report*, ed. T. Weekes, No. 385, p. 87.
26. G.D. Schmidt, R.H. Weymann, and C.B. Foltz (1989), "A Moderate-Resolution, High-Throughput CCD Channel for the Multiple Mirror Telescope Spectrograph," *Publications Astronomical Society of the Pacific*, Vol. 101, pp. 713–724, August 1989.
27. R. Howat, *et. al*. "Commissioning of and first results from the UIST imager spectrometer, *SPIE Astronomical Telescopes + Instrumentation*, 2004, Glasgow, UK.